VOL. 2, NO. 2, APRIL 2007 ISSN 1819-6608
ARPN Journal of Engineering and Applied Sciences


www.arpnjournals.com

# NUMERICAL STUDY OF OPPOSING MIXED CONVECTION IN A VENTED ENCLOSURE

M. M. Rahman[1], M. A. Alim[1], M. A. H. Mamun[2], M. K. Chowdhury[1] and A. K. M. S. Islam[3]
[1]Department of Mathematics, Bangladesh University of Engineering and Technology, Dhaka, Bangladesh
[2]Department of Mechanical Engineering, Bangladesh University of Engineering and Technology, Dhaka, Bangladesh
[3]Department of Mechanical and Chemical Engineering, Islamic University of Technology, Board Bazar, Gazipur, Bangladesh
E-mail: arifhasan@me.buet.ac.bd

## ABSTRACT

A numerical study has been performed on mixed convection in a vented enclosure by finite element method. An external fluid flow enters the enclosure through an opening in the left vertical wall and exits from another fixed opening in the right vertical wall. Various inlet port configurations are extensively studied with the change of governing parameters. For mixed convection, the significant parameters are Grashof number (*Gr*), Richardson number (*Ri*) and Reynolds number (*Re*) by which different fluid and heat transfer characteristics inside the cavity are obtained. In present study streamlines, isotherms, average temperature and average Nusselt number of the heated wall are reported for *Ri* = 0 to 10, *Re* = 50, 100 and 200; *Pr* = 0.71, 7.5 and 50 and different inlet position *Hi* = 0.05, 0.50 and 0.95. From the present analysis it is found that with the increase of Reynolds and Richardson numbers the convective heat transfer becomes predominant over the conduction heat transfer and the rate of heat transfer from the heated wall significantly depends on the position of the inlet port. Higher Nusselt number is observed at very large Prandtl number. Empirical correlations are developed to express the above relation mathematically.

**Keywords:** Mixed convection, finite element method, Richardson number, square enclosure, heat flux.

## INTRODUCTION

Thermal buoyancy forces play a significant role in forced convection heat transfer when the flow velocity is relatively small and the temperature difference between the surface and the free stream is relatively large. The buoyancy force modifies the flow and the temperature fields and hence the heat transfer rate from the surface. Problems of heat transfer in enclosures by free convection or combined free and forced convection have been the subject of investigations for many years. Mixed convection occurs in many heat transfer devices, such as the cooling system of a nuclear power plant, large heat exchangers, cooling of electronic equipment, ventilation and heat or pollution agent clearance. The relative direction between the buoyancy force and the externally forced flow is important. In the case where the fluid is externally forced to flow in the same direction as the buoyancy force, the mode of heat transfer is termed assisting combined forced and natural convection. In the case where the fluid is externally forced to flow in the opposite direction to the buoyancy force, the mode of heat transfer is termed opposing combined forced and natural convection or mixed convection.

Different orientations or heating conditions of the cavity as well as ventilation systems can induce different kinds of heated buoyant flows which enhance the heat transfer in different manners. For opposing mixed convection in cavity, when the buoyancy parameter is not large, the small amount of the buoyant flow induced along the heated wall can either aid or resist the main flow and cause either enhancement or reduction in the heat transfer. When the buoyancy parameter becomes large, the resulting heated buoyant flow along the side wall becomes substantial. Depending upon the flow position of the mainstream, the buoyant flow can cause different kinds of flow reversals which will alter the entire flow characteristic and enhance the heat transfer in different manners. For vertical enclosure, heating is usually from the side. Therefore, enhancement in the heat transfer can be obtained from the initial position of the main flow. This main flow is usually a cold forced flow which forms in mushroom shaped plumes associated with vortices. This kind of secondary flow is a laminar plume throughout the cavity and may have a transition into a two-dimensional convection rolls. The transition into different flows depends on the magnitudes of the Reynolds number and the buoyancy parameter. Therefore, it appears that the opposing mixed convection in a cavity with different orientations of ventilation system differs so drastically that studies on the flow and heat transfer in such a different system must be carefully performed in a separate manner.

Various researchers investigated the effect of mixed convective flows in enclosures using analytical, experimental and numerical methods. Arpaci and Larsen (1984) have presented an analytical treatment of the mixed convection heat transfer in tall cavities, which had one vertical side moving, other vertical boundaries at different temperatures and horizontal boundaries are adiabatic. They showed that in this particular case, the forced and buoyancy-driven parts of the problem could be solved separately and combined to obtain the general mixed convection problem.

Cha and Jaluria (1984) and Jaluria and Cha (1985) numerically studied mixed convection in a long horizontal cavity with inlet and outlet placed on the vertical walls in order to understand heat energy extraction process in a solar pond. Kumar and Yuan (1989) studied the laminar, two-dimensional mixed convection flow in a

rectangular enclosure with inlet and outlet ports. Papanicolaou and Jaluria (1990, 1993 and 1995) investigated mixed convection in a cavity with a localized heat source. Papanicolaou and Jaluria (1990 and 1993) reported that flow patterns generally consist of recirculating cells due to buoyancy forces generated by the heat source. An improvement in cooling can be also obtained when the outlet flow opening is placed near the bottom of the vertical wall. The results obtained by Papanicolaou and Jaluria (1995), in an inclined channel for turbulent flow show that the best performance in heat transfer is observed when the channel is in a vertical location. Mixed convection in a partially divided rectangular enclosure was studied numerically by Hsu *et al.* (1997). The simulation was extended for wide range of Reynolds and Grashof numbers. They indicated that the average Nusselt number and the dimensionless surface temperature depended on the location and height of the divider. Mixed convection in an inclined channel was presented by Choi and Ortega (1993). It was also shown that the best performance in heat transfer is observed when the channel is in a vertical location.

Experimental investigations of mixed convective flows have also been carried out by a number of researchers. Gau *et al.* (2000) performed experiments on mixed Convection in a horizontal rectangular channel with side heating whereas Joye (1996) compared experimental correlations in opposing flow mixed convection heat transfer inside a vertical tube. Raji and Hasnaoui (1998, 2000 and 2001) reported the results of a numerical study of air laminar mixed convection in a rectangular cavity, including radiation, for $10^3 \leq Ra \leq 5\times10^6$ and $5 \leq Re \leq 5{,}000$. A control-volume finite-element method, using triangular elements, was used to study transient mixed convection in an air-cooled cavity by Omri and Nasrallah (1999), for $0.1 \leq Ri \leq 18$, $10 \leq Re \leq 500$, including radiation. Later on, Singh and Sharif (2003) extended their works by considering six placement configurations of the inlet and outlet of a differentially heated rectangular enclosure whereas the previous work was limited to only two different configurations of inlet and outlet. More recently, Manca *et al.* (2003) worked out a numerical investigation of three different cases of mixed convection in a channel with an open cavity for various ratios of channel opening and cavity height and the range of governing parameters were $0.1 \leq Ri \leq 100$, and $Re = 100$ and 1000.

The current geometry of interest is a square vented cavity with one of the side walls heated uniformly and the other walls insulted. This geometry has the potential application in the cooling of electronic equipment. When the circuit boards with electronic circuits printed in one side of the walls are arranged in parallel with passage in between for cooling air moving horizontally, one will have the current configuration of cavity. Typical results on heat transfer for different inlet and outlet position configurations are discussed in previous literatures but limited to a fixed inlet/outlet positions. Hence, a suitable configuration of inlet and exit port locations can lead to a substantial enhancement of thermal performance. Besides, all earlier studies are reported for a fixed Prandtl number ($Pr$) value. Therefore, a systematic study on the mixed convection flow and the heat transfer is needed. The objective of this study to analyze the effects of Prandtl, Richardson and Reynolds numbers on the heat transfer characteristics of laminar mixed convection. The primary focus of this paper is the influence of inlet port locations on the surface heat transfer for a range of Richardson number, Prandtl number and Reynolds number. Both flow visualization and heat transfer measurements are performed to gain a good understanding of the physical process and to provide some useful data.

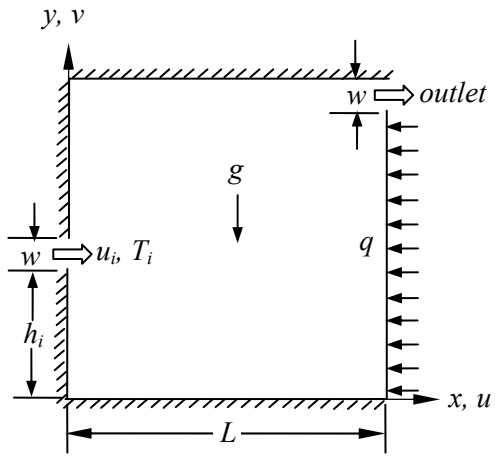


**Figure-1.** Schematic diagram of the problem considered and coordinate system.

## MODEL DESCRIPTION

Details of the geometry for the configuration are shown in Figure-1. The model considered here is a square cavity with a uniform constant heat flux $q$, applied on the right vertical wall. The cavity has dimensions of $L \times L$ and thus fixing the aspect ratio equal to 1. The other side walls including top and bottom of the cavity are assumed to be adiabatic. The inflow opening located on the left vertical wall is arranged as shown in the Figure 1 and may vary in location at a distance $h_i$ from the bottom of the enclosure. The outflow opening of the cavity is fixed at the top of the opposite heated wall and the size of the inlet port is the same size as the exit port which is equal to $w = 0.1L$. The inlet port location is altered along the left cavity wall with equal distance. In this case, the inlet port is situated in 19 locations in the vertical side wall of the cavity provided that in each simulation only one inlet port is considered. Consequently, after the simulation the inlet port location is moved a distance of $L/20$ away from its initial (lower) location and the simulation is repeated for the new location of the inlet port. It is assumed that the incoming flow is at a uniform velocity, $u_i$ and at the ambient temperature, $T_i$. Since the boundary conditions at the exit of the cavities are unknown, values of $u$, $v$ and $T$ are extrapolated at each iteration step, following a similar

approach to that used in the past by several authors [Papanicolaou and Jaluria (1990, 1993 and 1995); Hsu *et al.* (1997); Raji and Hasnaoui (1998, 2000 and 2001)]. All solid boundaries are assumed to be rigid no-slip walls.

## MATHEMATICAL FORMULATIONS

### Governing equations

Thermo physical properties of the fluid in the flow model are assumed to be constant except the density variations causing a body force term in the momentum equation. The Boussinesq approximation is invoked for the fluid properties to relative density changes to temperature changes, and to couple in this way the temperature field to the flow field. The governing equations for steady mixed convection flow using conservation of mass, momentum and energy can be written as

$$\frac{\partial u}{\partial x}+\frac{\partial v}{\partial y}=0 \quad (1)$$

$$u\frac{\partial u}{\partial x}+v\frac{\partial u}{\partial y}=-\frac{1}{\rho}\frac{\partial p}{\partial x}+\nu\left(\frac{\partial^2 u}{\partial x^2}+\frac{\partial^2 u}{\partial y^2}\right) \quad (2)$$

$$u\frac{\partial v}{\partial x}+v\frac{\partial v}{\partial y}=-\frac{1}{\rho}\frac{\partial p}{\partial y}+\nu\left(\frac{\partial^2 v}{\partial x^2}+\frac{\partial^2 v}{\partial y^2}\right)+g\beta\left(T-T_0\right) \quad (3)$$

$$u\frac{\partial T}{\partial x}+v\frac{\partial T}{\partial y}=\alpha\left(\frac{\partial^2 T}{\partial x^2}+\frac{\partial^2 T}{\partial y^2}\right) \quad (4)$$

with the boundary conditions

$u=u_i, v=0, and\ T=T_i$ at inlet

$v=0, p=0, \frac{\partial T}{\partial x}=0$ at the exit

$u=0, v=0\ and\ q=k\frac{\partial T}{\partial x}$ along the heated wall

$u=v=\frac{\partial T}{\partial x}=0$ along the vertical insulated wall,

$u=v=\frac{\partial T}{\partial y}=0$ along the horizontal insulated walls.

where x and y are the distances measured along the horizontal and vertical directions respectively; u and v are the velocity components in the *x*- and *y*-direction respectively; $T$ denotes the temperature; $\nu$ and $\alpha$ are the kinematics viscosity and the thermal diffusivity respectively; $p$ is the pressure and $\rho$ is the density; $q$ is the uniform constant heat flux.

Using the following dimensionless variables

$$X=\frac{x}{L}, Y=\frac{y}{L}, U=\frac{u}{u_i}, V=\frac{v}{u_i}, P=\frac{p}{\rho u_i^2}, \theta=\frac{T-T_i}{(qL/k)}$$

The governing equations (1) to (4) reduce to non-dimensional form:

$$\frac{\partial U}{\partial X}+\frac{\partial V}{\partial Y}=0 \quad (5)$$

$$U\frac{\partial U}{\partial X}+V\frac{\partial U}{\partial Y}=-\frac{\partial P}{\partial X}+\frac{1}{\mathrm{Re}}\left(\frac{\partial^2 U}{\partial X^2}+\frac{\partial^2 U}{\partial Y^2}\right) \quad (6)$$

$$U\frac{\partial V}{\partial X}+V\frac{\partial V}{\partial Y}=-\frac{\partial P}{\partial Y}+\frac{1}{\mathrm{Re}}\left(\frac{\partial^2 V}{\partial X^2}+\frac{\partial^2 V}{\partial Y^2}\right)+\frac{Gr}{\mathrm{Re}^2}\theta \quad (7)$$

$$U\frac{\partial \theta}{\partial X}+V\frac{\partial \theta}{\partial Y}=\frac{1}{\mathrm{Re}\,\mathrm{Pr}}\left(\frac{\partial^2 \theta}{\partial X^2}+\frac{\partial^2 \theta}{\partial Y^2}\right) \quad (8)$$

with the boundary conditions

Inlet: $U=1$, $V=0$, $\theta=0$

Exit: Convective boundary condition, $P=0$

At the cavity walls (except the right vertical wall):

$$U=V=\frac{\partial \theta}{\partial N}=0$$

At the heated right vertical wall: $U=V=0, \frac{\partial \theta}{\partial X}=-1$

Here $X$ and $Y$ are dimensionless coordinates varying along horizontal and vertical directions, respectively; $U$ and $V$ are dimensionless velocity components in the *X*- and *Y*-directions, respectively; $T$ is the dimensionless temperature; $P$ is the dimensionless pressure and $N$ is the non-dimensional distance in either $X$ or $Y$ direction acting normal to the surface.

In the above equations, the important governing parameters are as follows

Grashof number, $\mathrm{Gr}=\frac{\beta \mathrm{gqL}^4}{\upsilon^2 k}$, Prandtl number, $Pr=\frac{\upsilon}{\alpha}$, Reynolds number, $Re=\frac{u_i L}{\upsilon}$ and Richardson number, $Ri=\frac{Gr}{\mathrm{Re}^2}$.

The Reynolds number is based on the inlet velocity and the enclosure length whereas the Grashof number is based on the constant heat flux applied at the heated wall.

### Heat transfer calculations

The heat transfer calculation within the square enclosure is measured in terms of the average Nusselt number at the heated wall as follows

$$Nu = \frac{1}{L_s}\int_0^{L_s}\frac{h(y)y}{k}dy \quad (9)$$

where $L_s$ and $h(y)$ are the length and the local convection heat transfer coefficient of the heated wall respectively. An index of cooling effectiveness is the bulk average temperature defined as

$$\theta_{av} = \int \theta\, d\overline{V} / \overline{V} \quad (10)$$

where $\overline{V}$ is the cavity volume, which should be minimized.

**Computational procedure**

Numerical solutions for the governing equations with the associated boundary conditions were obtained using finite element techniques. A mixed finite element (FE) model is implemented, with two types of triangular Lagrange elements: an element with linear velocity and pressure interpolations for continuity and momentum equations and element with a quadratic basis velocity and temperature interpolations for energy equation. A stationary non-linear solver was used together with direct (UMFPACK) linear system solver [D. C. Lo et al. (2005), Roy and Basak (2005), Asaithambi (2003) and van Schijndel (2003)]. The relative tolerance for the error criteria was $10^{-4}$ and because the dependent variables vary greatly in magnitude, manual scaling of the dependent variable was used to improve numerical convergence. The manual scaling values are kept constant and were selected such that the magnitude of the scaled degrees of freedom was equal to one. The nonlinear equations were solved iteratively using Broyden's method with an LU-decomposition preconditioner, always starting from a solution for a nearby Richardson number. The numerical simulations were performed varying the number of elements of the grid in order to increase the accuracy and efficiency for the solutions. Non-uniform grids of triangular element were employed in the analysis, with denser grids clustering in regions near the heat sources and the enclosed walls.

**Grid sensitivity check**

Initially a grid sensitivity check is conducted to choose the proper grid for the numerical prediction. Five different types of grid are considered for the grid refinement analysis: 14313 nodes, 1986 elements; 24388 nodes, 3536 elements; 42913 nodes, 6386 elements; 70329 nodes, 10711 elements and 83304 nodes, 12600 elements. The deviations among the results are very little as shown in Table-1. Therefore the results of grid with 42913 nodes and 6386 elements are selected throughout the simulation.

**Table-1.** Grid sensitivity check at $Re$ = 100, $Ri$ = 10 and $Pr$ = 0.71

| **Nodes** (elements) | 14313 (1986) | 24388 (3536) | 42913 (6386) | 70329 (10711) | 83304 (12600) |
|---|---|---|---|---|---|
| **Nu** | 1.6087 | 1.6077 | 1.6077 | 1.6078 | 1.6078 |
| $\theta_{max}$ | 0.3669 | 0.3678 | 0.3680 | 0.3680 | 0.3679 |

**Code validation**

A computational model is validated for mixed convection heat transfer by comparing the results of correlation on mixed convection in ventilated cavity with uniform heat flux in left wall performed by Raji and Hasnaoui (1998). The right, top and bottom walls are insulated. In the present work numerical predictions have been obtained for Rayleigh number $10^6$ on the triangular mesh with 42913 nodes and 6386 elements for the same boundary condition of Raji and Hasnaoui (1998). Table-2 compares the present result with the result by Raji and Hasnaoui (1998). Figure-2 also shows the comparison of the flow and thermal fields between the present investigation and Raji and Hasnaoui (1998). The present result has a very good agreement with the results by Raji and Hasnaoui (1998). From these comparisons it can be decided that the current code can be used to predict the flow field for the present problem.

**Table-2.** Comparison of results for validations at $Re$ = 100, $H/D$ = 1/4 and $Pr$ = 0.72

| | **Present** | **Raji and Hasnaoui** (1998) |
|---|---|---|
| **Ra** | $10^6$ | $10^6$ |
| **Nu** | 1.702 | 1.691 |

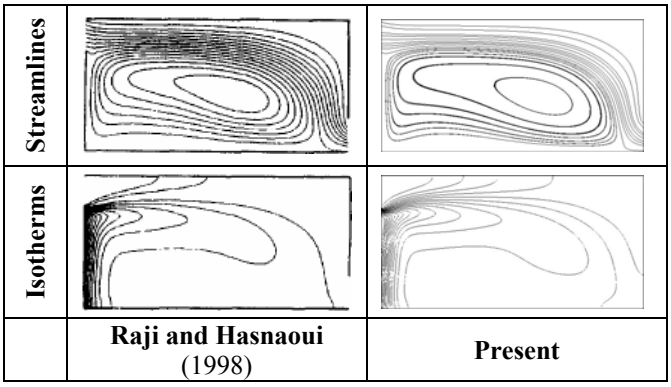


**Figure-2**. Comparison of streamlines and isotherms for validation at $Pr$ = 0.72, $Re$ = 100, $Ri$ = 1.0 with the results of Raji and Hasnaoui (1998).

**RESULTS AND DISCUSSION**

The simulations are carried out for mixed convection in a square cavity. The exit port of the cavity is fixed while the inlet port of the cavity is located at different positions in the cavity walls. The effects of the


inlet port locations, Reynolds number and Prandtl numbers on the heat transfer characteristics have been presented. The relative strength of the forced convection over natural convection can be judged on the base of *Ri*, in the mixed convection. In the case, as *Ri* approaches to unity, the buoyancy effect becomes important. Consequently, the natural convection dominates the mixed convection when $Ri > 1$. In the following, several cases related to the different configurations are compared in terms of streamlines, isotherms, average bulk fluid temperature and Nusselt numbers.

**Flow and thermal fields characteristics**

**Effect of relative inlet port location**

Figure-3 shows the streamlines and isotherms plot for various $H_i$. At the lowest inlet position, i.e. for $H_i = 0.05$ a jet-wall-type flow was observed similar to the one noticed in Singh and Sharif (2003) for similar values of *Re* and *Ri*. This is because the main flow penetrates into the cavity, exiting adjacent to the upper corner of the heat source. It can also be seen from Figure 3 (a1) that one circulating cell is formed over the main flow. For $H_i = 0.5$, two secondary circulating cells of same sizes are formed at the top and bottom of the inlet port as seen in Figure 3(b1). Thus for $H_i = 0.95$, Figure 3(c1) shows that one circulating cell is formed below the main flow. The formation of circulating cell is because of the mixing of the fluid due to buoyancy driven and convective currents. Similarly the isotherms inside the cavity are shown in the Figures 3(a2), 3(b2) and 3(c2) for the three different inlet port locations $H_i = 0.05$, 0.50 and 0.95 respectively. It is clear from these figures that the isotherms are almost same near the heated wall for the three different inlet port locations. Although a slightly thin thermal boundary is observed at low $H_i$, the corresponding isotherm plots do not significantly propagates from the heated surface.

**Effect of Richardson number**

Figures 4(a1) to (c1) show streamline plots for different values of *Ri* at $Re = 100$, $Hi = 0.2$ and $Pr = 0.71$. At low *Ri*, buoyancy effects are weak, and separation occurs at the opposite vertical wall of the heated surface. As *Ri* increases, buoyancy effects accelerated the fluid near the heated wall causing the recirculation near the bottom of the hot wall to disappear. This elimination of the separation region occurs between *Ri* of 0 and 10. The corresponding isotherm plots for the above cases are presented in Figures 4(a2) to (c2). As shown, the thermal boundary layer decreases in thickness slowly as the *Ri* increases. This is revealed by the denser concentration of isotherms near the bottom of the hot wall. In regions where flow separation begins due to lower *Ri*, the isotherms diverge reflecting a decrease in heat transfer associated with the onset of separation. However, despite this initial decrease in heat transfer following the acceleration of the upper recirculation with the increase of *Ri,* the temperature gradients and heat transfer increases rapidly.

**Effect of Prandtl number**

Representative streamline plots are displayed in Figure 5 (a1) to (c1) for different values of *Pr* at $Re = 100$, $Ri = 1.0$ and $H_i = 0.2$. At $Ri = 1.0$, the recirculation region at the upper-left corner is dominated by the adverse pressure gradient effects and the thinning of the thermal boundary layer with increasing *Pr* does not appear to greatly influence the separation region. As noted earlier, at $Pr = 0.71$, with increasing values of *Ri*, the flow near the heated surface is accelerated leading to the reduction of the separation along the bottom of the heated surface, and resulting in the appearance of the recirculation bubble towards the top of the heated wall. However, as *Pr* is increased, the corresponding decrease in the fluid conductivity limits the acceleration of the near hot- wall fluid to a thinner thermal boundary layer region. Therefore, the corresponding decreases in velocity away from the hot wall is also reduced and at $Pr = 50$ separation does not dominantly change on the opposite vertical wall. The corresponding isotherm plots are presented in Figure 5 (a2) to (c2). As expected, the thermal boundary decreases in thickness as *Pr* increases. This is reflected by the denser dustering of isotherms close to the hot wall as *Pr* increases. The spread of isotherms at low values of *Pr* is due to a strong stream wise conduction that decreases the stream wise temperature gradient in the fluid.

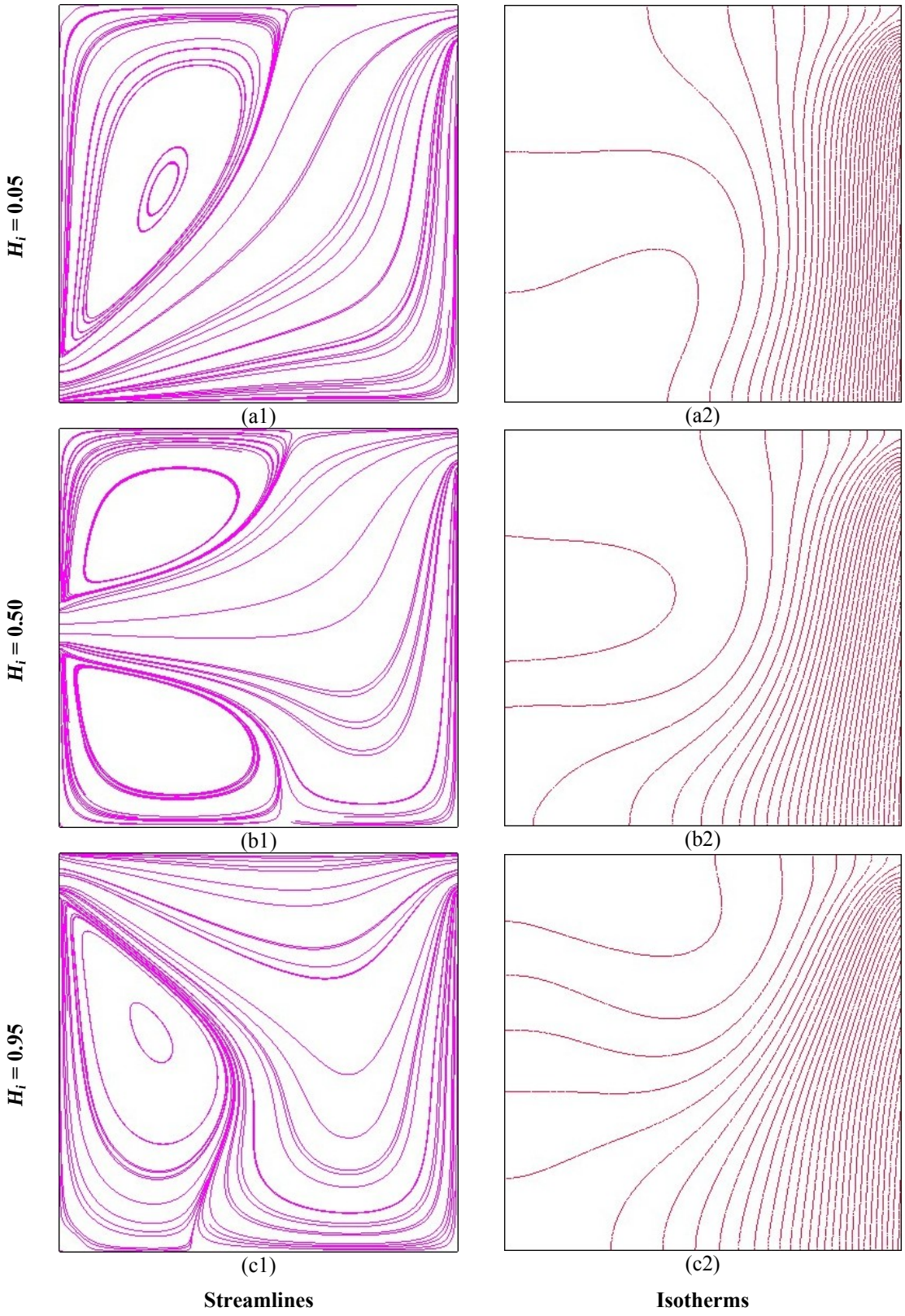


**Figure-3.** Streamlines and isotherms plot for different inlet position at $Ri = 1.0$, $Re = 100$ and $Pr = 0.71$.

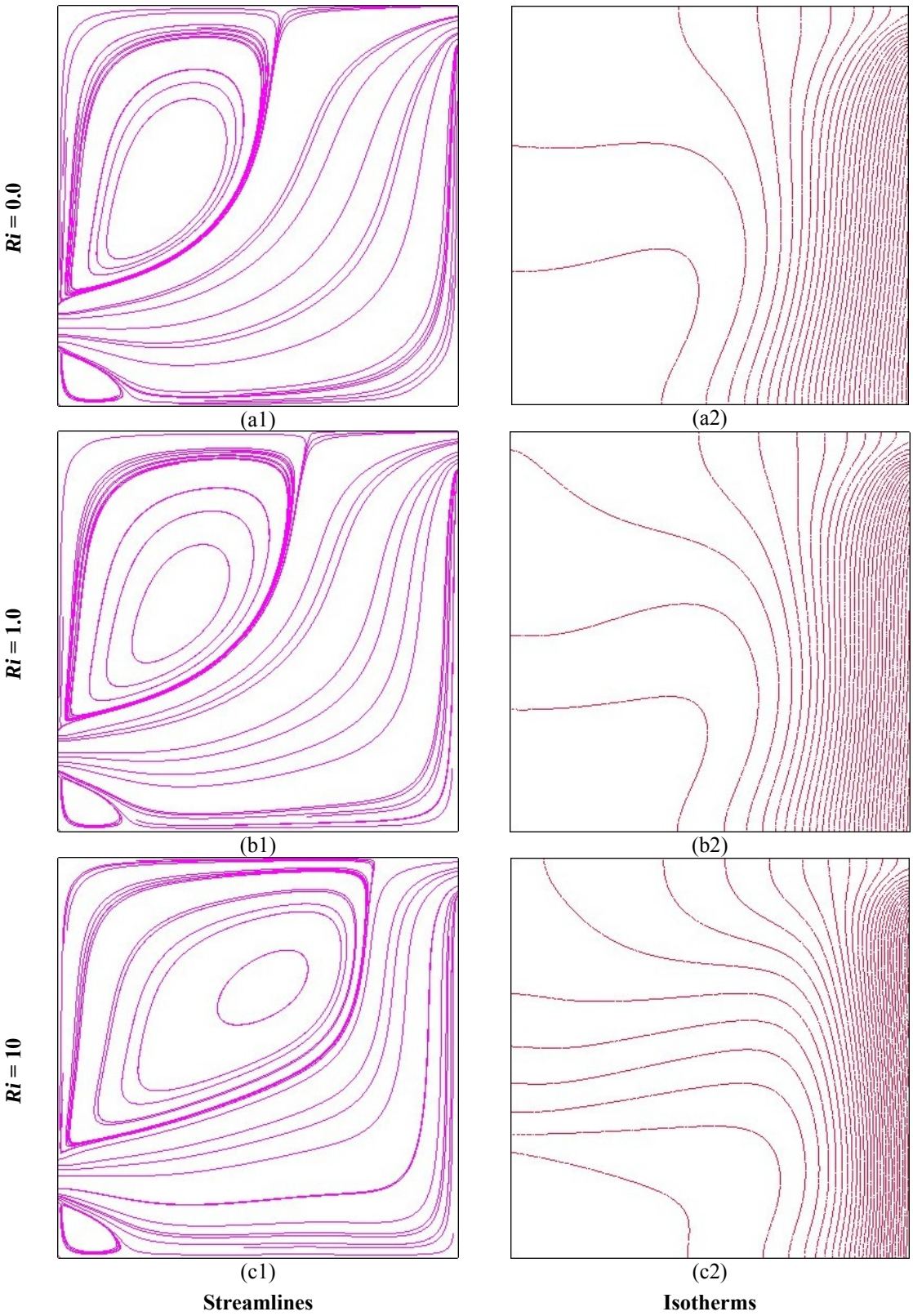


**Figure-4.** Streamlines and isotherms plot for different Richardson numbers at $H_i$ = 0.2, $Re$ =100 and $Pr$ = 0.71

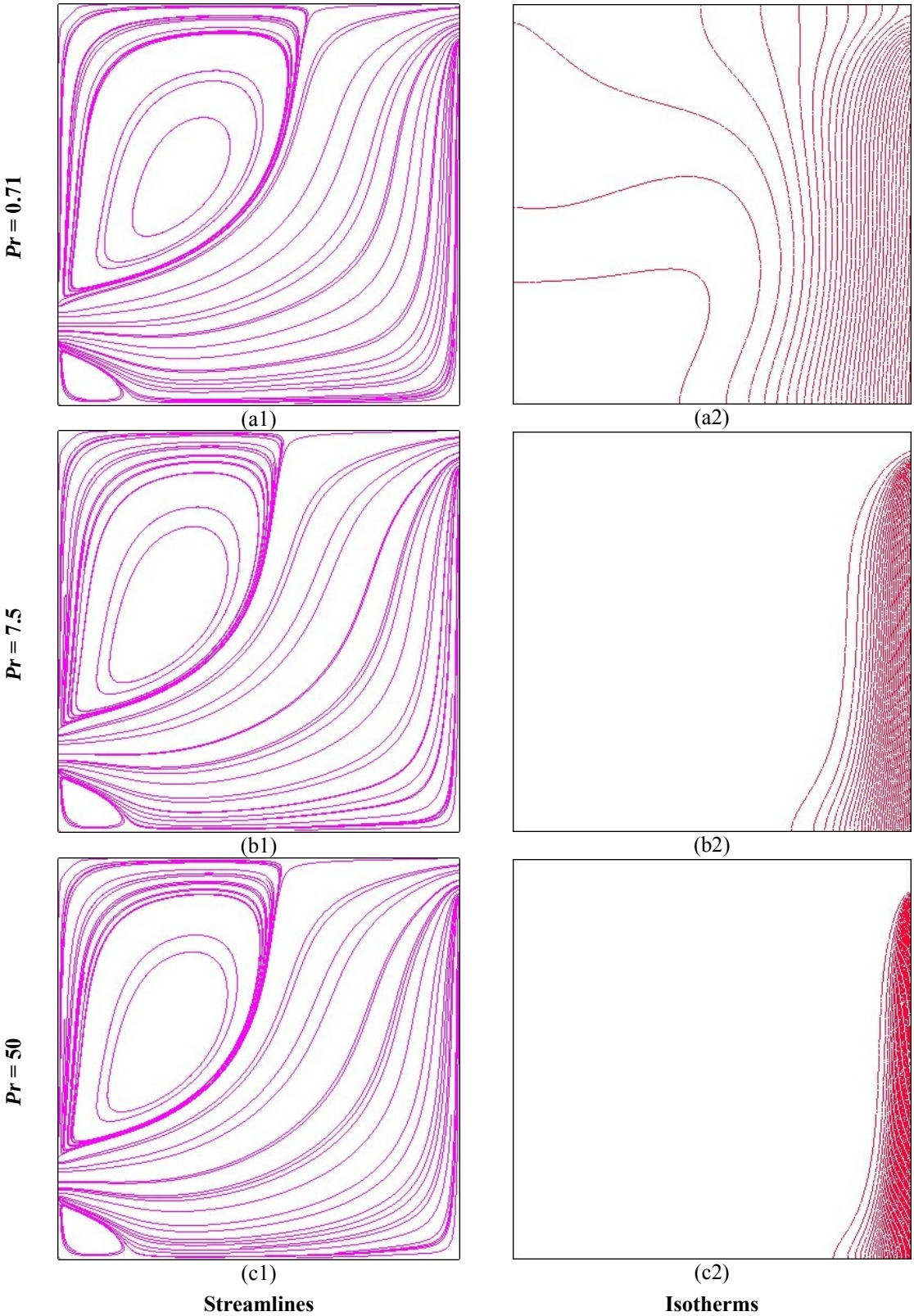


**Figure-5.** Streamlines and isotherms plot for different Prandtl numbers at $Ri = 1.0$, $Re = 100$ and $H_i = 0.2$

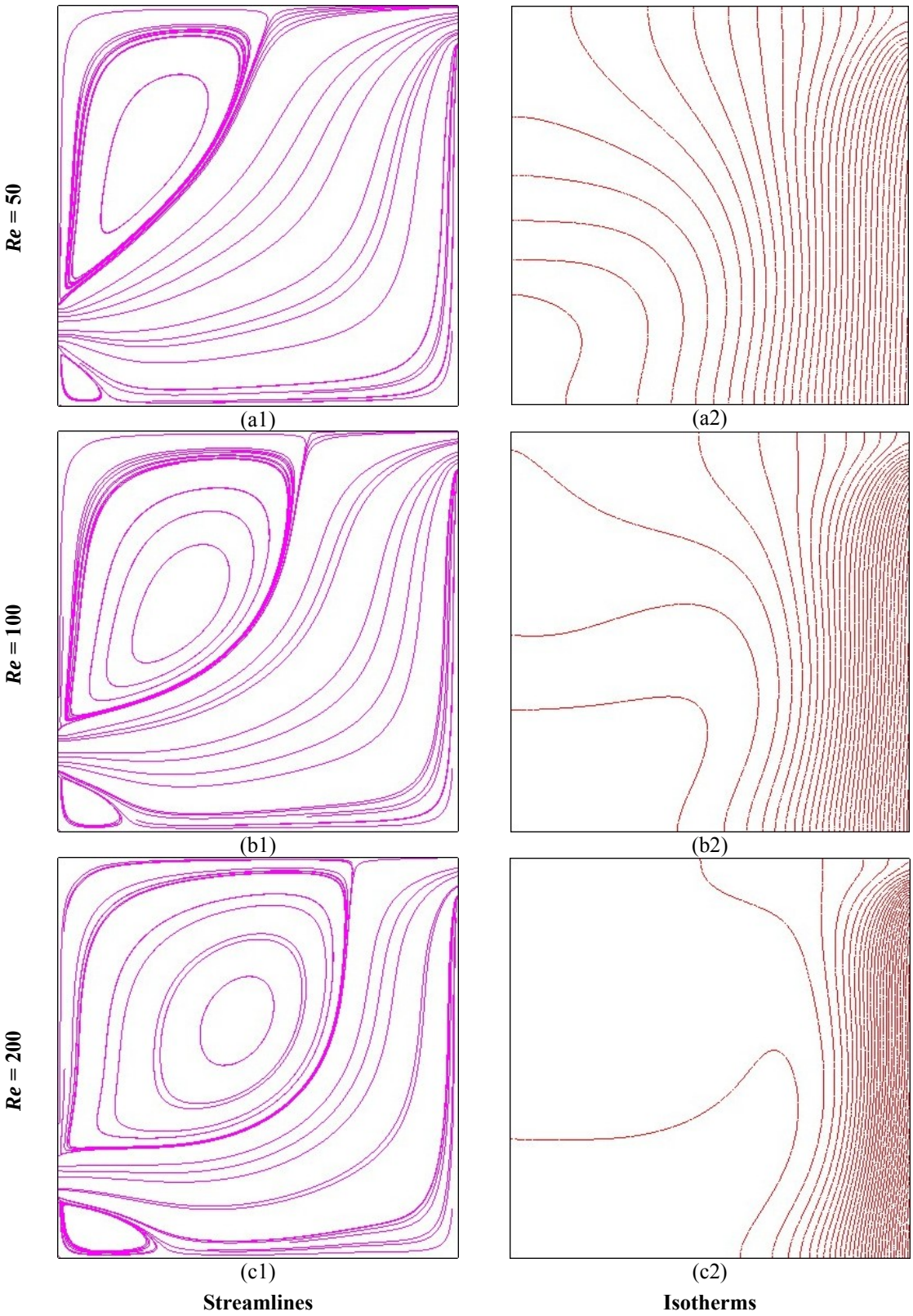


**Figure-6.** Streamlines and isotherms plot for different Reynolds numbers at $Ri = 1.0$, $Pr = 0.71$ and $H_i = 0.2$

**Effect of Reynolds number**

Now the attention is drawn to see the effect of increase of Reynolds number on the flow and temperature distribution in the square cavity. The streamlines and the isotherms at steady state for *Re* = 50, 100 and 200 are depicted, respectively, in Figures 6(a1) to (c1) and Figures 6(a2) to (c2) while *Ri* = 1.0 and *Hi* = 0.2. At smaller value of Re in Figure 6(a1) there exist two circulating cells of different sizes at the top and bottom of the inlet port. With the increasing value of *Re* The size of the two circulating cells gradually increases. Corresponding temperature distributions can be seen in Figures 6(a2) to (c2). It can be seen that increase in Re reduces the thermal boundary thickness and it is possible, since at larger value of *Re*, the effect of gravitation force becomes negligible.

**Heat transfer characteristics**

The heat transfer effectiveness of the enclosure is displayed in terms of average Nusselt number values and the dimensionless average bulk fluid temperature. The effect of varying $H_i$ on average Nusselt number along the hot wall are illustrated for different *Ri* in Figure-7 for a *Pr* value of 0.71. As the flow develops and the bulk fluid gets heated for low *Ri,* the Nusselt number profiles expectedly decrease from their higher values near the bottom inlet position to the upper inlet position. There always exists a maximum Nusselt number at $H_i$ = 0.2 for all values of *Ri* whereas a minimum value of *Nu* is expected to be found near the top position of the inlet port. In general, the level of *Nu* increases with *Ri* due to the thinning of the near-wall boundary layer and decrease of the average bulk fluid temperature. At *Ri* of 10, as seen in Figure-7, Nusselt number profile is almost constant with $H_i$ due to less separation observed near the heated wall.

Figure-8 illustrate the influence of *Pr* on the average temperature distribution for various *Ri.* Observing the temperature profile, no significant changes occurs with the increase of *Ri* for high value of *Pr* but for low *Pr* the average temperature decreases as $Ri \leq 4$ and increasing Pr has almost constant effect on $\theta_{av}$ for all value of $Ri > 4$. This is to be expected since *Pr* is an important parameter in the energy equation and its effects are always present independent of the magnitude of buoyancy forces. The reduction of average bulk fluid temperature as shown in Figure-8 is very much comparable with *Pr* between 0.71 and 1.0. This is because thermal boundary layer thickness decreases sharply initially for *Pr* = 0.71 to 1.0. Higher Pr implies lower thermal diffusion of heat from the heated surface and lower magnitudes of the buoyancy source term and buoyancy induced flow acceleration. This explains the difference in profiles obtained at high values of Ri for different values of *Pr*.

The overall heat transfer results (*Nu*) for different values of *Pr* in the square enclosure for $H_i$ = 0.2 are compared with the variation of *Ri* in Table 3. *Nu* increases significantly with increasing *Pr*, and is due to a decrease in the thermal boundary layer thickness with a consequent increase in the temperature gradient as *Pr* increases. Comparing the heat transfer rates from the heated wall inside the square enclosure with optimum inlet position ($H_i$ = 0.2), it is apparent that the average Nusselt numbers are higher only for high *Ri* and *Pr* values.

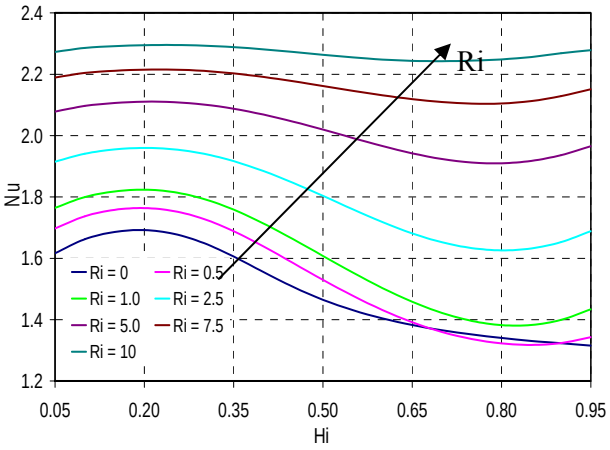


**Figure-7.** Variation of average Nusselt number as a function of inlet port location at different Richardson numbers.

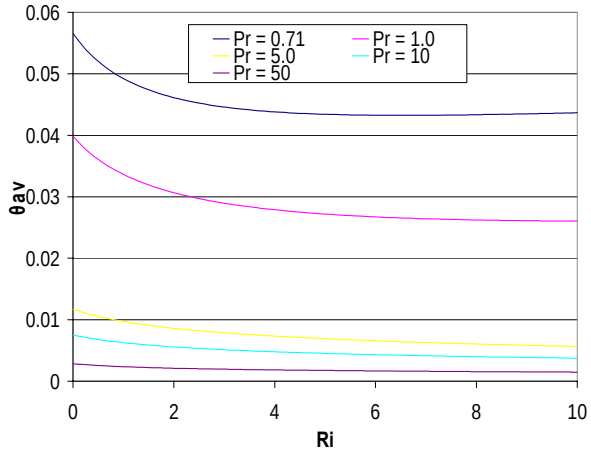


**Figure-8**. Variation of average temperature as a function of Richardson numbers at different Prandtl numbers.

**Table-3.** Effect of Prandtl and Richardson number on average Nusselt number of the heated wall.

| *Ri* | *Pr* = 0.71 | *Pr* = 1.0 | *Pr* = 7.5 | *Pr* = 10 | *Pr* = 50 |
|---|---|---|---|---|---|
| 0.0 | 1.692 | 1.953 | 4.060 | 4.489 | 6.920 |
| 0.5 | 1.764 | 2.032 | 4.145 | 4.574 | 6.997 |
| 1.0 | 1.824 | 2.099 | 4.222 | 4.650 | 7.069 |
| 2.0 | 1.920 | 2.209 | 4.355 | 4.784 | 7.200 |
| 5.0 | 2.111 | 2.436 | 4.659 | 5.092 | 7.513 |
| 7.5 | 2.215 | 2.568 | 4.853 | 5.290 | 7.721 |
| 10. | 2.295 | 2.671 | 5.016 | 5.457 | 7.900 |

Nusselt number as a function of Richardson number based on enclosure height for different Reynolds numbers is shown in Figure-9. Here three different trends of variation of average Nusselt number with the change of Richardson number are observed. When *Ri* increases from 0 to 10, the

average Nusselt number increases. This behavior results from the onset of thermal instabilities and the probable development of secondary flow due to uniform heating and forced flow, causes rapid mixing from the left to the right inside the enclosure.

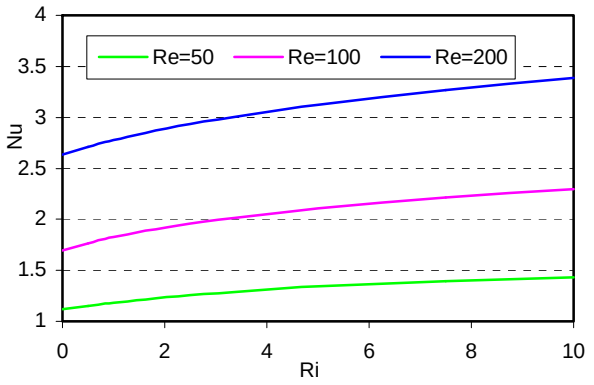


**Figure-9**. Variation of average Nusselt number with Richardson numbers.

**Heat transfer correlation**

The average Nusselt numbers shown in Figure-7 are mathematically correlated with the inlet port locations ($H_i$) for different Richardson numbers ($Ri$), Prandtl number ($Pr$) of 0.71 and Reynolds number ($Re$) of 100. The correlation can be written as

$$Nu = 0.0935\ Ri + 1.0118\ H_i + 0.0562\ Ri\ H_i + 0.0038\ Ri^2 - 4.2196\ H_i^2 - 0.0018\ Ri^3 + 3.5184\ H_i^3 + 0.0001 Ri^4 - 0.6254\ H_i^4 + 1.6304 \qquad R^2 = 99.5\% \qquad (11)$$

Similarly the mathematical correlation of the average Nusselt numbers shown in Table 3 with the Prandtl number ($Pr$) for different Richardson numbers ($Ri$), inlet port locations ($H_i$) of 0.2 and Reynolds number ($Re$) of 100 can be written as

$$Nu = 0.1757\ Ri^{0.7169} + 6.2096\ Pr^{0.1559} - 4.3447 \qquad R^2 = 99.5\% \qquad (12)$$

Lastly the mathematical correlation of the average Nusselt numbers shown in Figure 9 with the Reynolds number ($Re$) for different Richardson numbers ($Ri$), inlet port locations ($H_i$) of 0.2 and Prandtl number ($Pr$) of 0.71 can also be written as

$$Nu = 0.2612\ Re^{0.4883} + 0.1329\ Ri^{0.6395} - 0.7657 \qquad R^2 = 99.2\% \qquad (13)$$

Where $R^2$ is the maximum correlation coefficient.

## CONCLUSIONS

A numerical investigation on mixed convection in a square cavity was carried out using a finite element method. The present study examined and explained the complex interaction between buoyancy and force flow in a vented square enclosure with an inlet situated at the left edge of the vertical insulated wall, where the exit port is fixed at the top of the heated vertical surface. A total of nineteen inlet locations, shown in Figure-1, have been considered. The study encompasses a range of Reynolds number from 50 to 200, a range of Prandtl number from 0.71 to 50 and a range of Richardson number from 0 to 10. A detail investigation of the heat transfer in terms of fluid temperature and the average Nusselt number has been undertaken for different values of $H_i$, $Ri$, $Re$ and $Pr$. The following are some of the important observations made:
For $H_i$ = 0.2, higher heat transfer rate is always observed for all value of $Ri$. Also a minimum point exists at $H_i$ = 0.8.

For low $Ri$, the Nusselt number reaches a minimum near the onset of flow separation along the heated wall. This behavior is suppressed at high $Pr$. With the increase of $Ri$ since no flow separation exists along the heated wall, the behavior is more linear.

The effect of increasing Prandtl number on the total heat transfer is considerably greater than the effect of increasing $Ri$.

The numerical solutions indicate that increasing the value of $Re$ leads to higher heat transfer coefficient, higher heat source temperature, and higher intensity of recirculation.

## NOMENCLATURE

| | |
|---|---|
| $C_p$ | specific heat of the fluid at constant pressure ($Jkg^{-1}K^{-1}$) |
| $g$ | gravitational acceleration ($ms^{-2}$) |
| $Gr$ | Grashof number, $g\beta qL^4/\upsilon^2 k$ |
| $h$ | convective heat transfer coefficient ($Wm^{-2}K^{-1}$) |
| $h_i$ | inlet port location |
| $H_i$ | non-dimensional inlet port location |
| $w$ | height of the inflow and outflow openings (m) |
| $k$ | thermal conductivity of the fluid ($Wm^{-1}K^{-1}$) |
| $L$ | length of the cavity (m) |
| $L_s$ | length of the heated wall |
| $Nu$ | Average Nusselt number |
| $N$ | non-dimensional distance |
| $p$ | pressure ($Nm^{-2}$) |
| $P$ | non-dimensional pressure, $p/\rho u_i^2$ |
| $Pr$ | Prandtl number, $\upsilon/\alpha$ |
| $q$ | heat flux ($Wm^{-2}$) |
| $R$ | Correlation coefficient |
| $Ra$ | Rayleigh number, $Gr \cdot Pr$ |
| $Re$ | Reynolds number, $u_{i\,L}/\upsilon$ |
| $Ri$ | Richardson number, $Gr/Re^2$ |
| $T$ | temperature (K) |
| $\theta$ | non-dimensional temperature, $(T\text{-}T_i)/(q\ L/k)$ |
| $\theta_{max}$ | Maximum non-dimensional temperature |
| $\theta_{av}$ | average non-dimensional temperature |
| $u, v$ | velocity components ($ms^{-1}$) |
| $U, V$ | non-dimensional velocity components, $u/u_i$, $v/u_i$ |
| $\overline{V}$ | cavity volume |
| $x, y$ | Cartesian coordinates (m) |
| $X, Y$ | non-dimensional Cartesian coordinates, $x/L$, |

| | |
|---|---|
| | $y/L$ |
| Greek symbols | |
| $\alpha$ | thermal diffusivity, $k/\rho C_p$ ($m^2s^{-1}$) |
| $\beta$ | thermal expansion coefficient ($K^{-1}$) |
| $\rho$ | density of the fluid ($kgm^{-3}$) |
| $\upsilon$ | kinematic viscosity of the fluid ($m^2s^{-1}$) |
| Subscripts | |
| $av$ | average |
| $s$ | heated surface |
| $i$ | inlet state |
| max | maximum |

**ACKNOWLEDGEMENT**

The authors wish to acknowledge Department of Mathematics, Bangladesh University of Engineering and Technology, Dhaka, Bangladesh, for support and technical help throughout this work.

**REFERENCES**

Arpaci, V.S. and Larsen, P.S. 1984. Convection Heat Transfer, Prentice-Hall, 90.

Asaithambi, A. 2003. Numerical solution of the Falkner-Skan equation using piecewise linear functions, Applied Mathematical Computations. Vol. 81: 607-614.

Cha, C.K., and Jaluria, Y. 1984. Re-circulating mixed convection flow for energy extraction. International Journal of Heat and Mass Transfer. Vol. 27: 1801-1812.

Choi, C.Y., Ortega, A. 1993. Mixed convection in an inclined channel with a discrete heat source. Int. J. Heat Mass Transfer. Vol. 36(2): 3119-3134.

Gau, C., Jeng, Y.C., and Liu, C.G. 2000. An Experimental Study on Mixed Convection in a Horizontal Rectangular Channel Heated From a Side. ASME J. Heat Transfer. Vol. 122: 701–707.

Hsu, T.H., Hsu, P.T., How, S.P. 1997. Mixed convection in a partially divided rectangular enclosure. Numer. Heat Transfer, Part A. Vol. 31: 655-683.

Jaluria, Y., and Cha, C. K. 1985. Heat Rejection to Surface Layer of a Solar Pond. J. Heat Transfer. Vol. 107: 99-106.

Joye, D. D. 1996. Comparison of Correlations and Experiment in Opposing Flow, Mixed Convection Heat Transfer in a Vertical Tube with Grashof Number Variation. Int. J. Heat Mass Transfer. Vol. 39: 1033–1038.

Kumar, R., Yuan, T.D. 1989. Re-circulating mixed convection flows in rectangular cavities. AIAA J. Thermophys. Heat Transfer. Vol. 3: 321-329.

Lo, D. C., Young, D. L., and Lin, Y.C. 2005. Finite element analysis of 3-d viscous flow and mixed convection problems by the projection method. Numerical Heat Transfer, Part A. Vol. 48: 339-358.

Manca, O., Nardini, S., Khanafer, K., Vafai, K. 2003. Effect of Heated Wall Position on Mixed Convection in a Channel with an Open Cavity. Numerical Heat Transfer, Part A. Vol. 43: 259-282.

Omri, A., and Nasrallah, S. B. 1999. Control Volume Finite Element Numerical Simulation of Mixed Convection in an Air-Cooled Cavity, Numer. Heat Transfer, Part A. Vol. 36: 615-637.

Papanicolaou, E., and Jaluria, Y. 1990. Mixed Convection from an Isolated Heat Source in a Rectangular Enclosure. Numerical Heat Transfer, Part A. Vol. 18: 427-461.

Papanicolaou, E., and Jaluria, Y. 1993. Mixed Convection from a Localized Heat Source in a Cavity with Conducting Walls: A Numerical Study. Numerical Heat Transfer, Part A. Vol. 23: 463-484.

Papanicolaou, E., and Jaluria, Y. 1995. Computation of Turbulent Flow in Mixed Convection in a Cavity with a Localized Heat Source. ASME J. Heat Transfer. Vol. 117: 649-658.

Raji, A., and Hasnaoui, M. 1998. Mixed Convection Heat Transfer in a Rectangular Cavity Ventilated and Heated from the Side. Numer. Heat Transfer, Part A. Vol. 33: 533-548.

Raji, A., and Hasnaoui, M. 1998. Correlations on Mixed Convection in Ventilated Cavities. Revue Ge´ne´rale de Thermique. Vol. 37: 874-884.

Raji, A., and Hasnaoui, M. 2000. Mixed Convection Heat Transfer in Ventilated Cavities with Opposing and Assisting Flows. Engineering Computation, Int. J. Computer-Aided Eng. Software. Vol. 17(5): 556-572.

Raji, A., and Hasnaoui, M. 2001. Combined Mixed Convection and Radiation in Ventilated Cavities. Engineering Computation, Int. J. Computer-Aided Eng. Software. Vol. 18(7): 922-949.

Singh, S., and Sharif, M. A. R. 2003. Mixed Convective Cooling of a Rectangular Cavity with Inlet and Exit Openings on Differentially Heated Side Walls. Numerical Heat Transfer, Part A. Vol. 44: 233-253.

Van Schijndel, A. W. M. 2003. Modeling and solving building physics problems with FemLab, Building and Environment. Vol. 38: 319-327.